The Catalytic Cycle of Biosynthetic Thiolase: A Conformational Journey of an Acetyl Group through Four Binding Modes and Two Oxyanion Holes‡

Petri Kursula,§ Juha Ojala,§ Anne-Marie Lambeir,|| and Rik K. Wierenga*,§

Department of Biochemistry and Biocenter Oulu, P.O. Box 3000, FIN-90014 University of Oulu, Oulu, Finland, and Laboratory of Medical Biochemistry, University of Antwerp, Antwerp, Belgium

Received August 13, 2002; Revised Manuscript Received November 1, 2002

ABSTRACT: Biosynthetic thiolase catalyzes the formation of acetoacetyl-CoA from two molecules of acetyl-CoA. This is a key step in the synthesis of many biological compounds, including steroid hormones and ketone bodies. The thiolase reaction involves two chemically distinct steps; during acyl transfer, an acetyl group is transferred from acetyl-CoA to Cys89, and in the Claisen condensation step, this acetyl group is further transferred to a second molecule of acetyl-CoA, generating acetoacetyl-CoA. Here, new crystallographic data for *Zoogloea ramigera* biosynthetic thiolase are presented, covering all intermediates of the thiolase catalytic cycle. The high-resolution structures indicate that the acetyl group goes through four conformations while being transferred from acetyl-CoA via the acetylated enzyme to acetoacetyl-CoA. This transfer is catalyzed in a rigid cavity lined by mostly hydrophobic side chains, in addition to the catalytic residues Cys89, His348, and Cys378. The structures highlight the importance of an oxyanion hole formed by a water molecule and His348 in stabilizing the negative charge on the thioester oxygen atom of acetyl-CoA at two different steps of the reaction cycle. Another oxyanion hole, composed of the main chain nitrogen atoms of Cys89 and Gly380, complements a negative charge of the thioester oxygen anion of the acetylated intermediate, stabilizing the tetrahedral transition state of the Claisen condensation step. The reactivity of the active site may be modulated by hydrogen bonding networks extending from the active site toward the back of the molecule.

Thiolases are enzymes utilizing the unique thioester chemistry of coenzyme A (CoA)[1] derivatives. These CoA-binding enzymes exploit the increased chemical reactivity of the C−C and C−H bonds near the thioester group in their catalysis (*1*). Enzymes using CoA or CoA derivatives are vital in several biochemical pathways, which include both degradative and synthetic routes. The net effect observed in the reaction catalyzed by thiolase is the shortening or lengthening by two carbon atoms of an acyl chain that is covalently bound to CoA via a thioester linkage. The two-carbon units are either transferred to CoA or obtained from acetyl-CoA (Ac-CoA).

Thiolases have been divided into degradative (EC 2.3.1.16) and synthetic thiolases (EC 2.3.1.9). While this division is based on the originally described biological functions of different thiolases, the clear molecular characteristic differentiating the two groups is substrate specificity, defined to a large extent by differences in the size of the substrate-binding pocket (*2*, *3*). While synthetic thiolases can only use the short chain substrates acetyl-CoA and acetoacetyl-CoA (AcAc-CoA), degradative thiolases are also able to utilize longer chain substrates (*4*). Furthermore, synthetic thiolases are always tetrameric, but degradative enzymes can be either tetramers or dimers. Deficiencies in both degradative and biosynthetic thiolases have been linked to several human disease conditions (*5*−*7*). Recently, biosynthetic thiolases have also been objects of increasing commercial interest due to attempts to enzymatically create biodegradable plastic-like polymers (*8*). The same is true for other thiolase-related enzymes, such as polyketide synthases (*9*) and ketoacyl synthases (*10*). Here, we will focus on the details of the reaction mechanism of the biosynthetic thiolase (acetoacetyl-CoA thiolase) from *Zoogloea ramigera*.

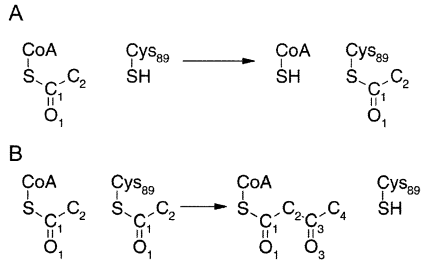

FIGURE 1: The two-step reaction catalyzed by thiolase. (A) Transfer of an acetyl group from Ac-CoA to Cys89. (B) The Claisen condensation step, in which the acetyl group from the acetylated enzyme is transferred to the second Ac-CoA molecule, resulting in the formation of AcAc-CoA. The numbering scheme for the atoms of the acetyl and acetoacetyl moieties is also introduced.

Biosynthetic thiolase catalyzes the biological Claisen condensation of two Ac-CoA molecules to form AcAc-CoA (Figure 1) (*4*, *11*). This is one of the fundamental pathways

‡ Coordinates and structure factors for the crystal structures presented in this paper have been deposited in the Protein Data Bank with the following entry codes: 1M3K for the unliganded C89A mutant, 1M3Z for the C89A mutant complexed with Ac-CoA, 1M4S for the acetylated unliganded thiolase, 1M4T for butyrylated thiolase, 1M1O for the C89A mutant complexed with AcAc-CoA, and 1M1T for the Q64A mutant.

* To whom correspondence should be addressed. Telephone: +358-(8)5531199. Fax: +358(8)5531141. E-mail: rik.wierenga@oulu.fi.

§ University of Oulu.

|| University of Antwerp.

[1] Abbreviations: Ac-CoA, acetyl-CoA; AcAc-CoA, acetoacetyl-CoA; CoA, coenzyme A; TLS, translation−libration−screw.

10.1021/bi0266232 CCC: $22.00
Published on Web 12/05/2002

of carbon chain assembly in vivo. Furthermore, it is the first step in many cellular biosynthetic pathways, including those which generate cholesterol, steroid hormones, and ketone bodies. The reaction is also used by certain microbes, such as *Z. ramigera*, as the first step in the synthesis of a polyester, poly-β-hydroxybutyrate (*12*). In addition, the reverse reaction, which can also be catalyzed by a synthetic thiolase when AcAc-CoA is the substrate, is crucial in the β-oxidation of fatty acids (*13*), as well as in the metabolism of ketone bodies (*14*).

The enzymological properties of *Z. ramigera* thiolase have been studied in great detail (*12*, *15*−*17*). The pH optimum of the enzyme is between 7.5 and 8.5 (*18*). The kinetic properties of the degradative and synthetic thiolases from pig heart and *Escherichia coli* have been investigated in detail (*4*, *19*). The kinetic properties of the degradative and biosynthetic thiolases are rather different (*4*, *20*): biosynthetic thiolase has 100-fold higher k_{cat} values than the degradative enzyme. However, the reaction mechanism is essentially the same. Thiolases have a classical ping-pong mechanism (*21*, *22*), which includes an acyl transfer step and a Claisen condensation step. The reaction involves the formation of a covalent acyl−enzyme intermediate, in which the active-site cysteine (Cys89 in the *Z. ramigera* thiolase) is acylated by an acyl-CoA molecule (*15*), after which CoA leaves the active site. Then, a molecule of Ac-CoA enters and is converted into 3-ketoacyl-CoA. In the case of biosynthetic thiolase, the net reaction converts two molecules of Ac-CoA into CoA and AcAc-CoA. Although the reaction is thermodynamically unfavorable (*15*), conditions in vivo, such as the excess of Ac-CoA, and the rapid removal of AcAc-CoA, allow the reaction to proceed to a significant degree.

Previously, crystallographic data for three key reaction intermediates of the biosynthetic thiolase from *Z. ramigera* have been presented (*3*, *20*). These structures included unliganded thiolase and acetylated thiolase complexed with CoA and acetyl-CoA (complexes 1, 3, and 5, respectively; Figure 2). In this study, we report the crystallographic analysis of the three remaining intermediates of the thiolase reaction cycle. An inactive mutant of *Z. ramigera* thiolase was constructed, in which the active-site cysteine 89 was replaced with an alanine, and its crystal structure was determined. This protein was used to determine the crystal structure of the complexes between thiolase and its natural substrates, Ac-CoA (complex 2) and AcAc-CoA (complex 6). The structure of unliganded wild-type biosynthetic thiolase, in which the active-site cysteine is acetylated, has also been obtained (complex 4). In addition, crystallographic experiments have been performed with the substrate analogue butyryl-CoA, and with another point mutant of thiolase, in which a dimer interface residue (Gln64) has been replaced with an alanine. The new data allow for a complete description of the structural events taking place at the thiolase active site during the catalytic cycle and highlight features of the catalytic cavity that are important for substrate specificity and catalysis.

EXPERIMENTAL PROCEDURES

Mutagenesis, Protein Purification, and Protein Characterization. The active-site residue Cys89 was replaced with alanine using the QuikChange site-directed mutagenesis kit (Stratagene, La Jolla, CA) according to the manufacturer's

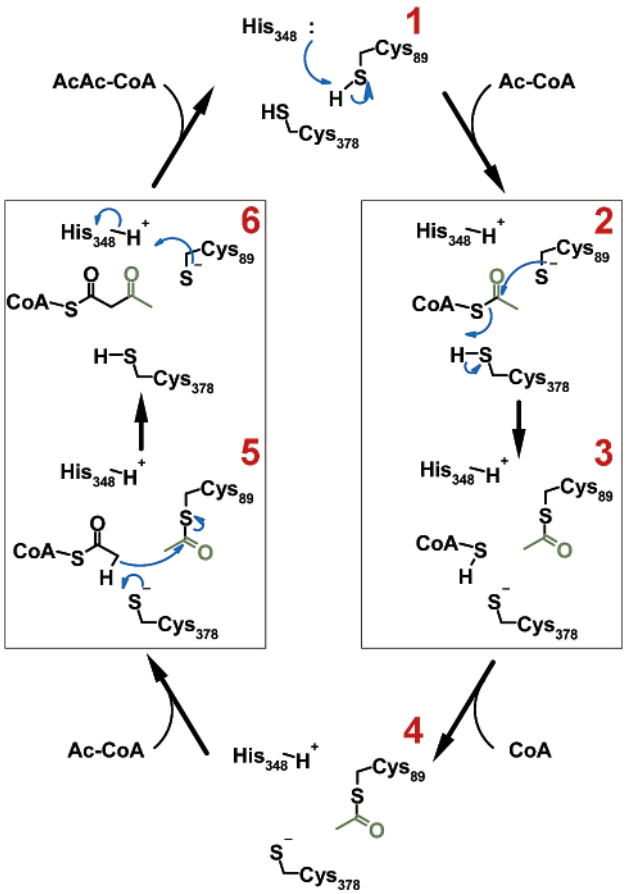

FIGURE 2: The thiolase reaction cycle. The six intermediates are shown and numbered in the synthetic (clockwise) direction from 1 to 6. The blue arrows indicate electronic rearrangements in the synthetic direction of the reaction. Detailed structural information about the complexes is depicted in Figure 6: complex 1 in Figure 6C, complex 2 in Figure 6A, complex 3 in Figure 6D, complex 4 in Figure 6C, complex 5 in Figure 6A, and complex 6 in Figure 6B. The acetyl group going through four distinct conformations is indicated in green. The two distinct chemical conversions are boxed: acyl transfer on the right and Claisen condensation on the left. The structural rearrangements during the reaction cycle are highlighted in Figure 7: the conversion of complex 2 to complex 3 in Figure 7A, the conformational changes of the acetylated cysteine (complexes 3−5) in Figure 7B, and the conversion of complex 5 to complex 6 in Figure 7C.

instructions. The oligonucleotide primers used for the mutagenesis (sense, 5′-GGCATGAACCAGCTTGCCGGCTC-GGGCCTGCGC-3′; antisense, 5′-GCGCAGGCCCGAGC-CGGCAAGCTGGTTCATGCC-3′) were obtained from TAG Copenhagen (Copenhagen, Denmark). Similarly, residue Gln64 was mutated into an alanine using suitable primers (sense, 5′-CCGGCCGGCGAAGGCGCGAACCCGGCCCG-CCAG-3′; antisense, 5′-CTGGCGGGCCGGGTTCGCGC-CTTCGCCGGCCGG-3′). Mutant clones were identified by cycle sequencing using the DYEnamic ET terminator kit (Amersham Biosciences, Espoo, Finland).

The expression and purification of the wild-type and mutant *Z. ramigera* biosynthetic thiolases were carried out as previously described for the wild-type enzyme (*3*). The protein was pure as assigned by SDS−PAGE (*23*) and Coomassie staining. Enzyme activities were measured in the direction of AcAc-CoA thiolysis, by following the loss of the Mg^{2+}−AcAc-CoA complex spectrophotometrically, as previously described (*15*). The C89A mutant had no detect-

Table 1: Currently Available Structures of *Z. ramigera* Biosynthetic Thiolase

description	growth and soaking conditions	ref	PDB entry
wild-type apoenzyme (complex 1)	grown in the absence of ligands	*20*	1DLU
C89A apoenzyme	grown in the absence of ligands	this work	1M3K
wild-type enzyme complexed with CoA	grown in the presence of 5 mM CoA, soaked for 30 s in 2.5 mM CoA[a]	*20*	1DLV
C89A complexed with Ac-CoA (complex 2)	grown in the absence of ligands, soaked for 10 min in 1 mM Ac-CoA[b]	this work	1M3Z
acetylated enzyme complexed with CoA (complex 3)	grown in the presence of 5 mM AcAc-CoA, soaked for 30 s in 2.5 mM AcAc-CoA[a]	*3*	1QFL
acetylated enzyme (complex 4)	grown in the absence of ligands, soaked for 30 s in 0.5 mM Ac-CoA, washed for 3 × 10 s without Ac-CoA[b]	this work	1M4S
butyrylated enzyme	grown in the absence of ligands, soaked for 10 min in 25 mM butyryl-CoA[b]	this work	1M4T
acetylated enzyme complexed with Ac-CoA (complex 5)	grown in the absence of ligands, soaked for 30 s in 2.5 mM Ac-CoA[a]	*20*	1DM3
C89A complexed with AcAc-CoA (complex 6)	grown in the absence of ligands, soaked for 5 min in 10 mM AcAc-CoA[b]	this work	1M1O
Q64A mutant	grown in the absence of ligands	this work	1M1T

[a] The soaking solution included the cryoprotectant. [b] The crystals were treated briefly with cryoprotectant after the described soaking experiment.

able thiolytic activity toward AcAc-CoA. The Q64A mutant was active toward AcAc-CoA, the k_{cat} being approximately 30% lower than that of the wild-type enzyme. The folding and thermal stability of the wild-type and mutant proteins were also studied by CD spectroscopy using a Jasco J-715 spectropolarimeter (Jasco, Tokyo, Japan). No significant differences were observed in the behavior of the wild-type and mutant proteins during expression, purification, and crystallization. CD spectroscopy also indicated that the variants were properly folded and had melting curves similar to those of the wild-type enzyme.

Crystallization. Wild-type and C89A mutant biosynthetic thiolases were crystallized as previously described for the wild-type enzyme (*3*). Briefly, both proteins produced diffraction-quality crystals in 1−3 days using either the hanging drop or the sitting drop vapor diffusion method at room temperature. The well solution contained 0.1 M sodium citrate (pH 5.0), 1.0 M Li_2SO_4, 0.9 M $(NH_4)_2SO_4$, 1 mM ethylenediaminetetraacetic acid, 1 mM dithiothreitol, and 1 mM NaN_3, and the protein concentration in the drop was 2 mg/mL. Slightly different conditions had to be used to crystallize the Q64A mutant. The protein concentration in the drop was 1 mg/mL, and the well solution contained 0.1 M sodium citrate (pH 5.5 or 6.0), 1.0 M Li_2SO_4, 1.1 M $(NH_4)_2SO_4$, 1 mM ethylenediaminetetraacetic acid, 1 mM dithiothreitol, and 1 mM NaN_3. All protein crystals were grown in the absence of ligands.

Data Collection and Processing. Prior to the treatment with cryoprotectant and crystallographic data collection, the crystals were soaked in substrate solutions (see Table 1). To obtain structures for the enzyme in complex with its natural substrates, the C89A mutant crystals were soaked for 10 min in a drop of well solution containing either 10 mM AcAc-CoA or 1 mM Ac-CoA. For the structure of the wild-type acetylated enzyme without the bound substrate, the crystals were first soaked in 0.5 mM Ac-CoA in well solution for 30 s. Subsequently, the crystals were washed three times for 10 s by transferring them three times to new drops of well solution in the absence of Ac-CoA. To obtain the structure of wild-type thiolase with a C4 substrate, the wild-type thiolase crystals were soaked for 5 min in a drop of the well solution containing 25 mM butyryl-CoA. The nomenclature of the structures of the studied intermediates is summarized in Figure 1.

The crystals were then prepared for crystallographic data collection by quickly soaking them in a drop of well solution containing the corresponding substrate and 24% glycerol as a cryoprotectant. The crystals were flash-frozen in a stream of gaseous nitrogen cooled to 100 K. The detailed protocols of the soaking experiments are listed in Table 1. All crystallographic data were collected at beamline I711 (*24*) of MAX-Lab (Lund, Sweden), except for the data for the apo form of the C89A mutant, which were collected at beamline ID29 at the ESRF (Grenoble, France). As previously discussed, the biosynthetic thiolase crystals exhibit strong anisotropic disorder (*3*). Thus, the data were collected using oscillation angles of 0.3−0.4°, and data processing was carried out using XDS (*25*). The data processing statistics are presented in Table 2. Five percent of the reflections were set aside for the calculation of R_{free} (*26*), and were thus not used in refinement.

Structure Solution, Refinement, and Validation. Since the unit cell dimensions did not change significantly from those previously observed (Table 2), the structure solution was initiated by performing rigid body refinement with REFMAC5 (*27*) of the CCP4 program package (*28*), using the previously determined structure of unliganded biosynthetic thiolase [PDB (*29*) entry 1DLU (*20*)] as the starting model. There is one thiolase homotetramer in an asymmetric unit. Each of the four subunits was defined as a separate rigid body. Subsequently, translation−libration−screw (TLS) refinement was performed in combination with restrained isotropic refinement using REFMAC5 (*27*, *30*). The two tight dimers, A−B and C−D subunit pairs, were defined as separate rigid bodies during TLS refinement. Noncrystallographic symmetry restraints were also applied between the four subunits, and during the late stages of refinement, only the restraints between the A−C and B−D subunit pairs were kept. Residues involved in crystal contacts were not included in the noncrystallographic symmetry restraints. Water molecules were added iteratively using ARP/wARP (*31*). Substrate and solvent molecules, as well as extra atoms at the modified residue Cys89 in the wild-type enzyme, were only added if they were clearly visible in the electron density

Table 2: Data Collection and Refinement Statistics

	acetylated thiolase	C89A with Ac-CoA	C89A with AcAc-CoA	butyrylated thiolase	C89A apo	Q64A
data collection statistics[a]						
resolution range (Å)	50−1.87 (1.95−1.87)	50−1.87 (1.95−1.87)	50−1.95 (2.05−1.95)	50−1.77 (1.80−1.77)	50−1.70 (1.80−1.70)	50−1.94 (2.00−1.94)
$I/\sigma(I)$	9.5 (3.2)	8.8 (2.9)	7.0 (2.9)	9.0 (2.6)	10.5 (2.5)	8.0 (2.9)
completeness (%)	97.9 (90.1)	90.8 (93.3)	99.6 (99.1)	99.1 (95.9)	90.0 (56.7)	97.5 (93.5)
redundancy	3.3 (2.6)	3.0 (2.8)	3.2 (3.1)	3.1 (2.3)	3.3 (2.1)	2.8 (2.2)
R_{sym} (%)	9.2 (35.4)	8.0 (35.3)	11.8 (36.4)	9.7 (34.4)	7.9 (32.9)	10.0 (28.3)
space group	$P2_1$	$P2_1$	$P2_1$	$P2_1$	$P2_1$	$P2_1$
unit cell parameters						
a, *b*, *c* (Å)	84.40, 79.28, 148.48	84.60, 79.68, 149.32	84.22, 79.22, 148.29	84.35, 79.31, 147.32	84.37, 79.20, 148.86	84.47, 78.95, 148.29
α, *β*, *γ* (deg)	90, 92.2, 90	90, 92.8, 90	90, 92.5, 90	90, 94.0, 90	90, 92.3, 90	90, 92.6, 90
refinement statistics						
resolution range (Å)	20−1.87	20−1.87	20−1.95	20−1.77	20−1.70	20−1.94
no. of reflections	158300	148800	141522	187094	193695	140595
no. of working set reflections	151113	141952	135151	178447	184714	134240
R factor (%)	20.6	19.2	21.1	20.6	19.9	19.9
no. of test set reflections	7187	6848	6371	8647	8981	6355
R_{free} (%)	24.7	24.2	25.8	24.2	24.3	24.5
no. of protein atoms	11368	11292	11284	11298	11336	11324
no. of substrate molecules	0	4	2	0	0	0
no. of water molecules	1094	1052	1002	1091	1159	1177
no. of sulfate molecules	4	4	4	4	4	4
no. of glycerol molecules	4	0	0	2	2	4
geometry statistics						
rmsd for bond distances (Å)	0.016	0.017	0.018	0.018	0.019	0.020
rmsd for bond angles (deg)	1.5	1.6	1.6	1.6	1.7	1.8
rmsd for *B* factors (Å^2)						
main chain	2.3	2.5	2.4	2.1	2.4	2.3
side chain	3.0	2.9	2.6	2.7	3.4	3.2
average *B* factors (Å^2)[b]						
protein atoms (A, B, C, D)	14, 14, 11, 13	20, 20, 22, 23	15, 15, 15, 15	14, 14, 14, 15	13, 13, 15, 16	11, 11, 9, 11
substrate atoms (A, B, C, D)	−	63, 65, 84, 89	48, 46, −, −	−	−	−
solvent atoms	41	45	43	42	40	39
Ramachandran plot (all subunits, %)						
most favored	90.2	92.0	89.8	90.3	91.4	90.4
additionally allowed	9.5	7.7	9.9	9.3	8.0	9.2
generously allowed	0.3	0.3	0.2	0.4	0.6	0.3
disallowed	0.0	0.0	0.1	0.0	0.0	0.2
noncrystallographic symmetry (A−C, B−D)						
rmsd for protein atoms (Å)	0.21, 0.22	0.19, 0.18	0.21, 0.23	0.21, 0.21	0.21, 0.21	0.25, 0.24
rmsd for *B* factors (Å^2)	3.4, 3.3	3.0, 3.3	2.6, 2.8	3.1, 3.4	3.0, 3.4	2.6, 2.7

[a] The values in parentheses correspond to the highest-resolution shell. [b] The contribution of the TLS parameters is not included in the *B* factors.

maps. The presence of the expected mutations in the C89A and Q64A variants was confirmed by the electron density maps. The quality of the protein models was checked with PROCHECK (*32*). The refinement and validation statistics are shown in Table 2. All further analysis concentrated on the B subunit, which is always best defined in the synthetic thiolase crystal structures.

RESULTS

Overall Description of the Molecule. The thiolase tetramer is, in fact, a dimer of tight dimers (Figure 3A). Each subunit of the thiolase tetramer consists of three domains: an N-terminal domain (residues 1−118 and 250−272) and a C-terminal domain (residues 273−392) having similar topology and a loop domain, which is an insertion of approximately 130 residues (residues 119−249) within the N-terminal domain after strand *β*4. The N- and C-terminal domains assemble into a five-layered α−*β*−α−*β*−α structure, with two central helices, termed Nα3 and Cα3, covered on each side by layers of *β*-strands and α-helices. The *β*-strands of the N-terminal domain and the C-terminal domain have the same topology of a mixed five-stranded *β*-sheet (*33*). In this *β*-sheet, strand *β*5 runs antiparallel to the other strands, *β*1 and *β*3 are at the edges of the sheet, and the assembly of the strands in the *β*-sheet is *β*1−*β*5−*β*4−*β*2−*β*3. *β*-Strands 2, 4, and 5 are completely buried in the bulk of the protein. The loop domain circles around the active site and is important for binding the CoA moiety of the substrate. In addition, residues 122−142 of the loop domain extend away from the subunit, interacting with the corresponding residues of the other subunits and thus forming the tetramerization motif (*3*) (Figure 3A,B).

The structures in this study were refined at resolutions ranging from 1.70 to 1.95 Å (Table 2). Residues 3−392 of all subunits could be built in all structures. In the Q64A and C89A mutant structures, as well as in the structure of the acetylated enzyme, Ser1 and Thr2 could also be included in the model. Ramachandran plots indicate that the only residues found in the generously allowed or disallowed regions are Leu88 and Asn65. Both of these residues are very well defined in the electron density maps, Leu88 being the residue next to the active-site Cys89, and Asn65 being located at the tight dimer interface, near Gln64 which points into the active site of the opposing subunit (Figure 3B). There are

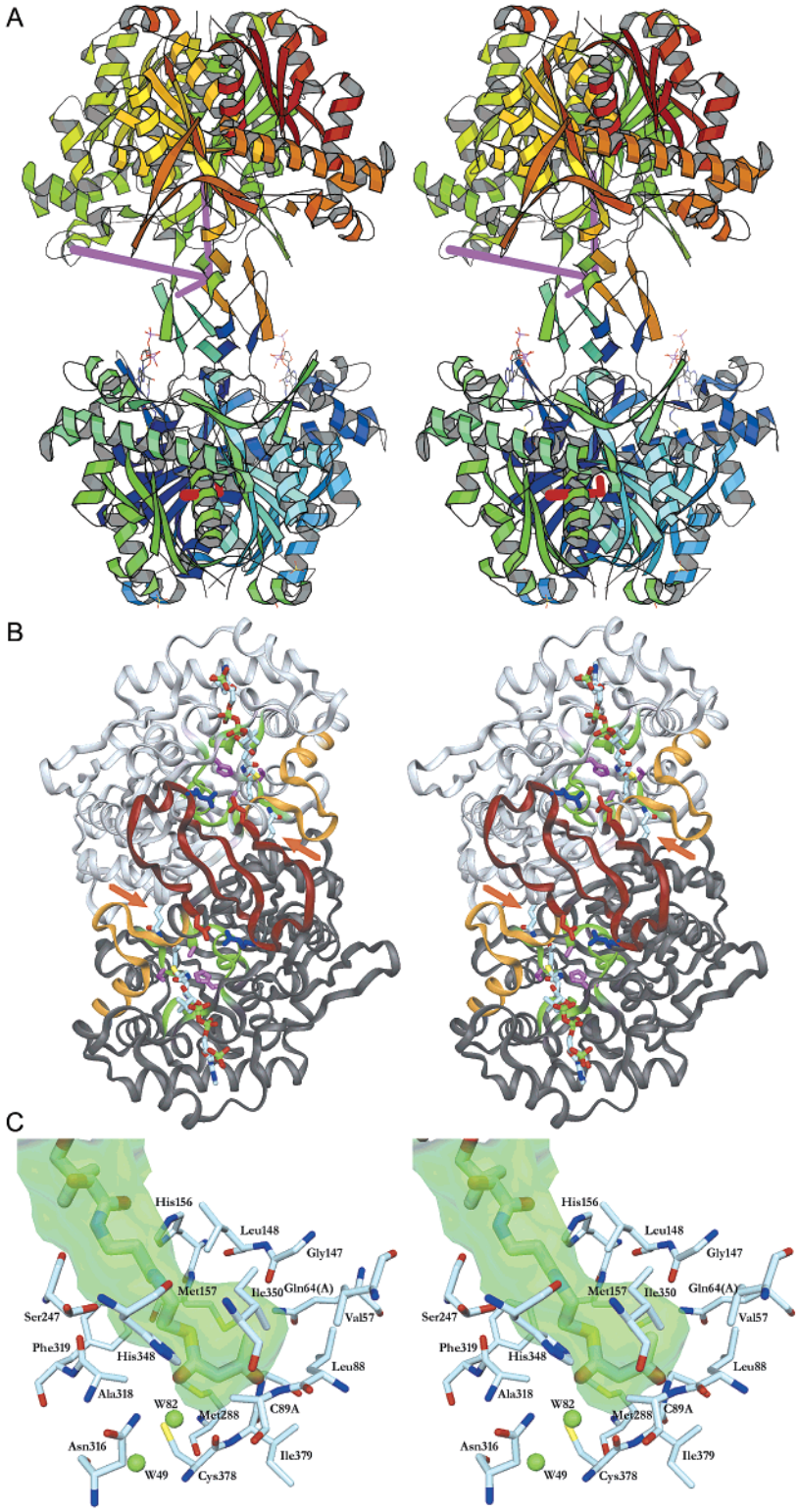

FIGURE 3: (A) Thiolase tetramer, which is a dimer of two tight dimers. Subunits A and B (below) are in blue−green colors, and subunits C and D (above) are in yellow−red colors. The libration axes of the TLS refinement for the two tight dimers are also shown (red axes for the A−B dimer and purple axes for the C−D dimer), as are two molecules of AcAc-CoA in the active sites of subunits A and B. The structure of complex 5, the C89A mutant thiolase complexed with AcAc-CoA, was used to prepare this figure and Figure 5. The image was made with Molscript (*47*). (B) A−B dimer viewed from the top. Subunit A (above) has a lighter gray color than subunit B. The tetramerization motif is red, and the loop region which becomes less ordered in the Q64A mutant is orange. The position of Gln64 is indicated by an orange arrow. The mode of binding of AcAc-CoA is also shown, and the three catalytic residues are indicated with purple. Four green main chain regions highlight the loop regions defining the bottom of the active-site cavity. Also in green is the region near Ser247, whereas the orange main chain defines the ceiling of the active-site pocket (see the text). The red and blue side chains refer to Asp141 and Arg129, which form a salt bridge between opposing subunits at both ends of the tetramerization loop. The image was made with DINO (*48*). (C) Substrate-binding cavity of biosynthetic thiolase (side view). The surface is the solvent-accessible surface calculated for the protein, including well-defined solvent molecules, in the absence of AcAc-CoA, which is bound in the active site. The image was made with MSMS (*49*) and DINO (*48*).

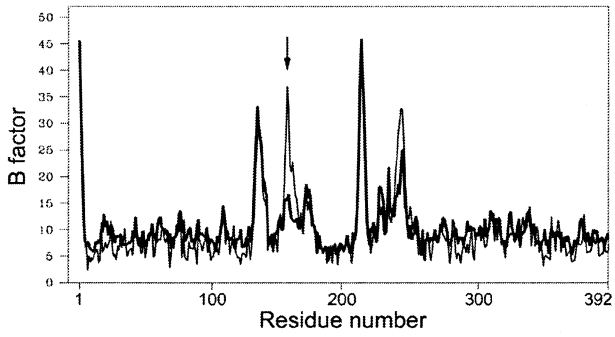

FIGURE 4: *B* factor plot, calculated using main chain atoms, for the unliganded thiolase mutants C89A (thick line) and Q64A (thin line). The B subunit of the tetramer was used for the analysis. It can be seen that while both variants have three regions of high isotropic *B* factors, the Q64A mutant has a fourth less ordered region, covering residues 147−163 of the loop domain (arrow). The *B* factors of the C89A mutant resemble closely those of the wild-type enzyme, both in the presence and in the absence of ligand (data not shown). The contributions of the TLS parameters are not included in the values.

three regions of high *B* factors both in the presence and in the absence of ligand, corresponding to loop regions near residues 136, 207, and 235 of each subunit (Figure 4). All these regions are within the loop domain, pointing into the interdimer space toward the opposing dimer and its active sites.

Due to crystal packing, the A−B dimer is much better defined in the electron density maps than the C−D dimer, and the previously described structures (*3*, *20*) had very high *B* factors for subunits C and D. The B subunit was used for the analysis of the structures, but all the discussed structural features are also visible in the A subunit. Contrary to previous structure refinements of this biosynthetic thiolase, TLS parameters (*30*) were used in the current refinement (Figure 3A). In the final structures, the individual isotropic *B* factors in all four subunits are low and very similar (Table 2), indicating that the parameters of TLS refinement account very well for the anisotropic disorder of the crystal, when the A−B and C−D dimers are used as separate rigid bodies during refinement. Figure 3A illustrates the libration axes for the two tight dimers, and it can be seen that a center of movement for the C−D dimer is found at the tetramerization motif.

Description of the Active Site. The active site of each thiolase subunit faces the interdimer space, not being blocked by crystal contacts (Figure 3A). The catalytic function of thiolase is performed by the protein atoms surrounding a cavity (Figure 3C). The bottom of this cavity is formed by four stretches of the polypeptide chain, leading into the two central helices (Nα3 and Cα3) of the thiolase fold and out of the two central strands (Cβ2 and Cβ4) of the second β-sheet (Figure 3B). This region is sealed off from bulk solvent by residues 147−156 of the loop domain, and by Gln64 of the adjacent subunit (Figure 3B).

The active site can only be reached via a narrow tunnel (Figure 3C), lined by the hydrophilic residues His156 and Ser247, which has two alternate conformations in all of the structures. These residues are located near the beginning and end of the loop domain, respectively, and this is the region binding the phosphopantetheine moiety of CoA. In all liganded structures of thiolase, the binding mode of the CoA portion is the same. In the presence of CoA, the volume of the remaining cavity at the active site is 80 Å^3, and no water molecules are detectable [PDB entry 1DLV (*20*)]. The cavity is lined by hydrophobic side chains from residues Val57, Leu88, Leu148, Met157, Met288, Phe319, and Ile350. Deepest in the cavity are the polar side chain of Gln64 of the opposing subunit of the tight dimer and an oxyanion hole formed by the main chain nitrogens of Cys89 and Gly380.

Central in the active-site cavity are the side chains of the catalytic residues Cys89 and Cys378, and toward the entrance of the cavity is the third catalytic residue, His348 (Figure 3). In the apo form of the wild-type enzyme, Sγ(Cys89) points toward O (378), where $\chi_1 = -34°$ [PDB entry 1DLU (*20*)]. Once a ligand binds [PDB entry 1DLV (*20*)], it rotates slightly ($\chi_1 = -58°$) toward His348, and it remains in this position throughout the catalytic cycle. The His348 side chain is anchored by a hydrogen bonding contact with Ser353 [the Nδ1(His348)−Oγ(Ser353) distance being 2.6 Å], which is an integral part of a buried water cluster. Sγ(Cys378) is in a somewhat strained conformation; for example, $\chi_1 = 67°$ (*3*, *20*). In this conformation, Sγ(Cys378) is close to N(Cys378) and O(Cys378), which are at a distance of 3.3 and 3.4 Å, respectively. During the catalytic cycle, Sγ(Cys378) does not rotate; it is kept in its position by the nearby Met288 and Gln322 residues. The Sγ(Cys378)−Sδ(Met288) and Sγ(Cys378)−Cδ(Gln322) distances are both 3.8 Å. Met288 and Gln322 anchor the Cys378 side chain in a fixed position, as they do not allow any rotation about χ_1. In this position, Sγ(Cys378) is hydrogen-bonded to Wat49 (3.3 Å) and Wat82 (3.5 Å). Sγ(Cys378) is 6 and 7 Å from Sγ(Cys89) and Nϵ2(His348), respectively.

Another important feature of the active site is the presence of hydrogen bonding networks leading from the catalytic center toward the back of the molecule (Figure 5). Two main networks can be distinguished, one on each side of strand Cβ2 of the β-sheet of the C-terminal domain, both being packed between a nearby helix and this β-strand. One network starts from Wat82. Wat82 is an integral part of the active site, being present in all unliganded and liganded structures. This network is indeed a 15 Å long water channel of seven water molecules connected to bulk solvent on the other side of the protein. The water molecules of this network interact with both side chain and main chain atoms. The other network extends away from active-site residues His348 and Asn316. This hydrogen bonding network is dominated by a cluster of six buried water molecules which interact with the buried charged side chains of Glu314 and Arg356. The central β-strand of the C-terminal β-sheet (Cβ2) contributes a buried charged residue to both networks, Glu314 and Glu317 (Figure 5). The third buried charged residue, Arg356, is part of the Cα3 helix.

The potential importance of Wat82 is highlighted by the fact that it is hydrogen bonded to catalytically crucial atoms of all three catalytic residues, in particular to Sγ(Cys378), Sγ(Cys89), and Nϵ2(His348). It is also hydrogen bonded to Wat49 and O(Cys378). These six atoms form a polar face of the active-site cavity, centered around Wat82, which is contacted from the interior of the protein by the Asn316 side chain through a hydrogen bond between Nδ2(Asn316) and Wat82. In the liganded structures, the thioester oxygen of both acetyl-CoA and acetoacetyl-CoA contacts the center of this face through a hydrogen bond with Wat82, further

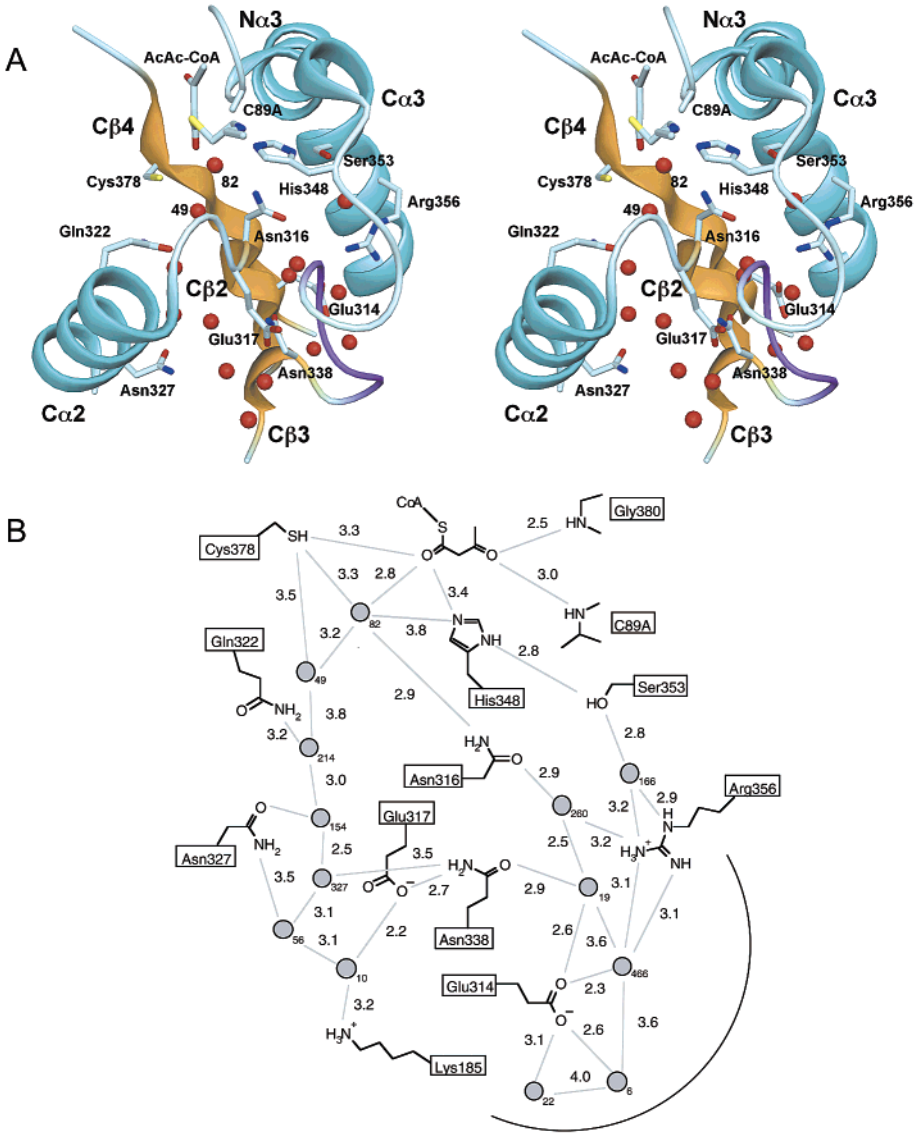

FIGURE 5: (A) Two water-mediated hydrogen bonding networks extend from the active site toward the back of the molecule, one on each side of the central β-sheet (view similar to that in Figure 3B). The loop formed by residues 339−342, shown in purple, seals one of the water networks away from bulk solvent. The channel on the left links the active site to bulk solvent, while the cluster on the right does not directly contact bulk solvent. The image was made with DINO (*48*). (B) Schematic representation of the hydrogen bonding networks. For clarity, only the interactions involving the water molecules and the side chain atoms of the protein are shown.

emphasizing the central position of Wat82 (see, for example, Figures 5 and 6).

Binding Mode of Acetyl-CoA. To be able to study the mode of binding of the natural substrates of thiolase, acetyl-CoA and acetoacetyl-CoA, the inactive mutant C89A was expressed, purified, and crystallized. Analysis of the crystal structure of the apo form of the C89A mutant protein indicated that the only significant difference in the structure of the mutant compared to the wild-type enzyme was the loss of the Sγ atom of Cys89. In addition, one extra water molecule is present in the active site of the mutant in the unliganded state and in the presence of Ac-CoA, being located in the oxyanion hole formed by the backbone N atoms of Cys89 and Gly380. Thus, the C89A mutant crystals were suitable for use in substrate soaking experiments.

The natural substrates of thiolase, Ac-CoA and AcAc-CoA, were soaked into crystals of the inactive C89A mutant thiolase, using the protocols described in Table 1. The crystal structures indicate that both substrates were bound in the active site of the mutant enzyme. The binding mode of the CoA part was similar for both substrates, and the same as that seen in previous complexes (*3*, *20*). Few direct contacts are present between the ADP moiety of the CoA molecule and the enzyme. This is in agreement with the earlier observations that CoA analogues, from which the 3′-phospho-ADP moiety has been removed, are also substrates for biosynthetic thiolase (*34*).

The first step in the thiolase reaction in the synthetic direction is the binding of Ac-CoA in the active site. The binding of Ac-CoA to the inactive enzyme (complex 2) is only slightly different from its binding to the acetylated intermediate (Figure 6A). In both structures, the thioester oxygen atom of Ac-CoA is hydrogen bonded to Nϵ2(His348), but in the C89A mutant complex, the thioester oxygen is somewhat rotated into the space created by the absence of the Sγ atom of Cys89. The CP2−SP1−C1−O1 dihedral

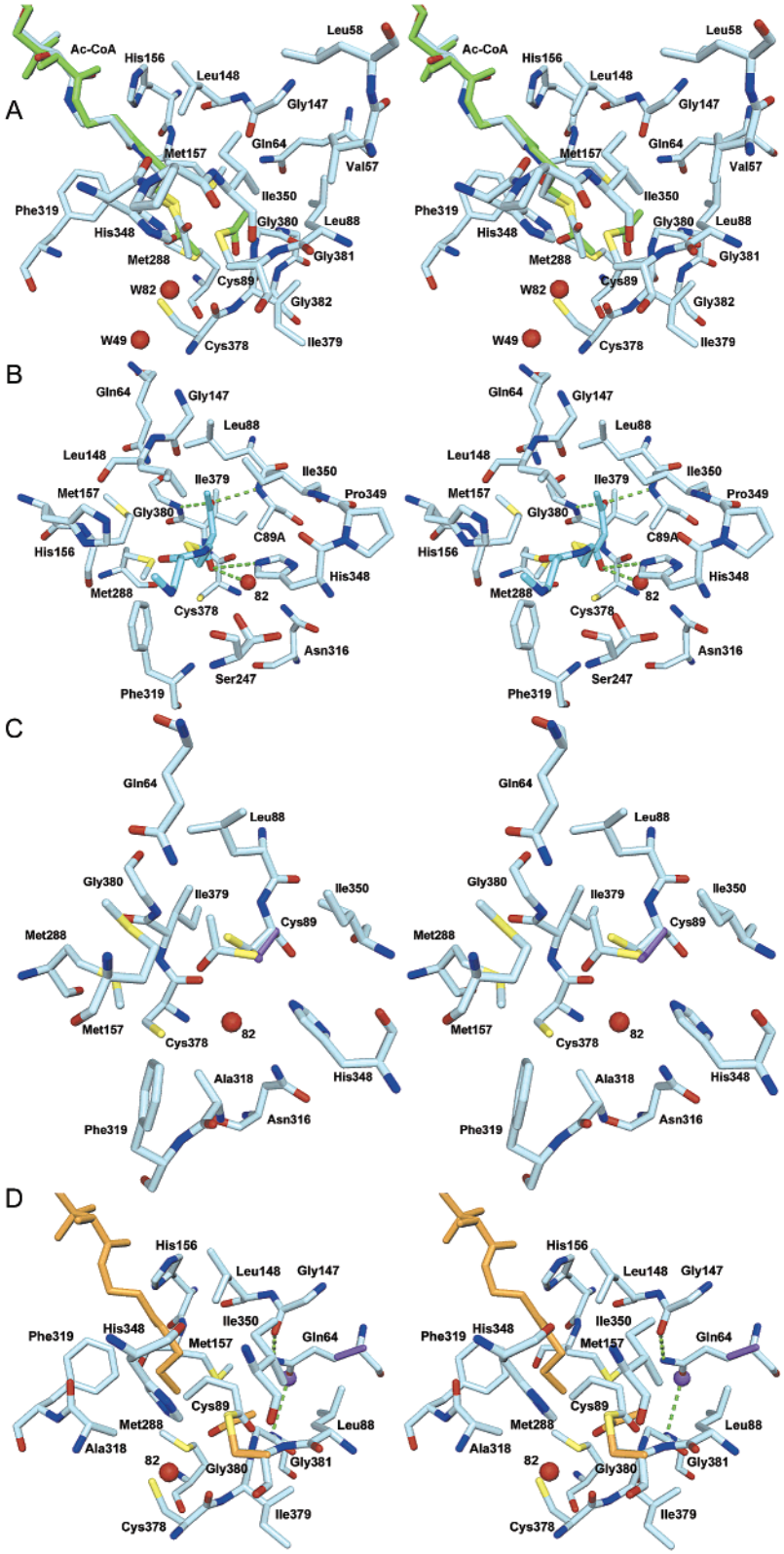

FIGURE 6: Specific structural features of the complexes. The numbering scheme for the complexes is defined in Figure 2. (A) Two structures complexed with Ac-CoA (complexes 2 and 5). The carbon atoms of complex 5 (Ac-Cys89 and Ac-CoA) are colored green. (B) Binding mode of acetoacetyl-CoA (complex 6, top view). Hydrogen bonding interactions of the thioester oxygen and the 3-keto oxygen of the acetoacetyl moiety with the polar atoms of oxyanion holes are indicated with dashed lines. (C) Structure of the acetylated enzyme (complex 4). Cys89 exists in two alternative conformations, one of which is acetylated and the other of which corresponds to the apo form (complex 1). Shown is also the conformation (purple) of Cys89 in the complex with CoA (*20*). (D) Structure of the butyrylated enzyme. Superimposed are CoA and Cys89 from complex 3 (in orange), demonstrating that butyrylation of Cys89 prevents the entry of a CoA molecule or its thioester derivative into the active site. Highlighted are also two hydrogen bonds made by the side chain of Gln64 in the wild-type enzyme (dashed lines), and the corresponding alanine residue and a water molecule replacing the side chain in the Q64A mutant (purple).

angles of Ac-CoA are −41° and 3° for complexes 2 and 5, respectively, indicating that in complex 5, the acetyl group is strained, while in complex 2, it adopts a more relaxed conformation. The C2 atom of Ac-CoA contacts the side chains of Met288 and Cys378, as well as O(Cys378) (Figure 6A). Presumably, in the wild-type enzyme, the binding mode of acetyl-CoA is very similar to that observed in the mutant. Energy minimization of the active site after the Sγ atom has been added back to Cys89 results in only small shifts such that the acetyl moiety of Ac-CoA rotates into a position more similar to that seen in complex 5 (unpublished results). It should also be noted that in the wild-type enzyme, the binding of CoA in the active site induces a rotation of approximately 30° about the Cα−Cβ bond of Cys89, resulting in the movement of Sγ(Cys89) toward Nϵ2(His348) (*20*). The Sγ atom of Cys89 now becomes a powerful nucleophile; this is crucial for the subsequent catalytic steps.

Binding Mode of Acetoacetyl-CoA. In the degradative direction, synthetic thiolase uses AcAc-CoA as its first substrate. The acetoacetyl group is almost planar in the structure of the C89A mutant complexed with AcAc-CoA (complex 6; see Figure 6B). The O1−C1−C2−C3 and C1−C2−C3−O3 dihedral angles are −177° and −160°, respectively. Consequently, both O1 and O3 atoms point away from the sulfur atom of CoA, toward the oxyanion holes formed by Wat82 and Nϵ2(His348) and N(Cys89) and N(Gly380), respectively (Figure 5B). The S and C4 atoms of the *S*-acetoacetyl moiety point upward, away from the catalytic residues and toward the side chain of Leu148 in the loop domain. This particular stretch of the loop domain is fixed in its position by a hydrogen bond between Nϵ2(Gln64) of the adjacent subunit and O(Gly147) (Figures 3B and 6D). C4 also points toward the Val57, Leu88, and Ile350 side chains, while the thioester sulfur atom is twisted toward the side chains of Met157, Met288, and Phe319 (Figures 3C and 6B).

The very tight and rigid cavity of the active site of biosynthetic thiolase directs the substrate into the proximity of the catalytic groups in the protein. The O3 atom of the acetoacetyl group points deep into the oxyanion hole formed by N(Cys89) and N(Gly380), while the O1 thioester oxygen is hydrogen bonded to Wat82 and Nϵ2(His348). Energy minimization of the structure after adding the Sγ atom to Cys89 results in only small changes in the conformation of the acetoacetyl group (unpublished results).

Unliganded Acetylated Thiolase. Crystals of wild-type thiolase were used to determine the structure of the covalently modified intermediate in the absence of bound substrate. Soaking of wild-type thiolase crystals in acetyl-CoA resulted in the formation of an acetyl−enzyme intermediate, which could be trapped in the absence of bound CoA or its derivatives due to careful washing of the crystals after soaking. Soaking in Ac-CoA produced an enzyme acetylated at Cys89 (complex 4). Upon refinement, it became evident that the structure is a mixture of the acetylated cysteine and an unmodified cysteine (Figure 6C) in the same conformation found in unliganded thiolase (*20*). This was expected, as the acetylated enzyme is hydrolyzed by water, and the half-life of the acetyl group on Cys89 in acetylated thiolase is only 2 min (*35*). After the acetyl group had been built in, extra electron density could be detected in the position where the Sγ atom of unliganded thiolase Cys89 is located. In refinement, occupancies of 50% were used for the overlapping conformations of modified and unmodified Cys89.

The orientation of the acetyl moiety of the acetylated cysteine in complex 4 is the same as in complex 3 (Figure 7B). The orientation of the acetyl moiety in complex 4 is such that the thioester oxygen points to the solvent, whereas the methyl group points to the cavity wall, in particular, Leu88 (Figure 6C). The thioester oxygen atom is hydrogen bonded to Wat82 (3 Å) and N(Gly380) (3.7 Å); in complex 3, there is an additional hydrogen bond to S(CoA) (3 Å).

Binding Studies with Butyryl-CoA. Butyryl-CoA was found to be only a weak inhibitor of the thiolysis of AcAc-CoA at 1 mM butyryl-CoA, despite the structure being very similar to both Ac-CoA and AcAc-CoA. Soaking of the C89A mutant crystals in 10 mM butyryl-CoA did not result in a detectable level of binding of the compound in the crystal structure (unpublished results), further indicating a low affinity of synthetic thiolase for butyryl-CoA. Crystallographic data indicate that soaking of wild-type thiolase crystals in butyryl-CoA results in Cys89 being butyrylated, with no additional CoA being bound (Figure 6D). The thioester oxygen of the butyrylated Cys89 points deep into the oxyanion hole of N(Cys89) and N(Gly380). In this mode of binding, the Cβ(Cys89)−Sγ(Cys89)−C1−O1 dihedral angle is strained (−10°), as also seen for the acetyl group on Cys89 (28°) in the structure of complex 5 (*20*).

Following acyl transfer in the crystal, the tightness of the active site results in a conformation of the transferred butyryl group that sterically prevents further entry of a CoA molecule (Figure 6D), in good agreement with the narrow substrate specificity of the enzyme. It is clear that in thiolases with longer chain length specificity, the acyl group must adopt a conformation different from that observed for the butyryl group, to allow the further entrance of CoA or Ac-CoA.

Structure of the Q64A Mutant. Gln64 is a highly conserved residue in biosynthetic thiolases. It is located at the dimer interface, and its side chain points toward the active site of the adjacent subunit of the tight dimer, interacting with residues of this opposing monomer (Figures 3B and 6D). Nϵ2 of Gln64 is hydrogen bonded to the main chain carbonyl oxygen of Gly147 of the loop domain, and it is also very close (3.6−3.7 Å) to the Sδ and Cϵ atoms of Met157. The Oϵ1 atom, on the other hand, is hydrogen bonded to N(Gly381). The Q64A mutant was purified and crystallized (Table 1). The protein is enzymatically active in the thiolysis of AcAc-CoA, the experimental k_{cat} being slightly smaller than that for the wild-type enzyme. The overall structure of the Q64A mutant is essentially the same as that of the wild-type enzyme, except for the absence of the side chain of Gln64 (Figure 6D). One extra water molecule is detected in the cavity induced by the mutation; this water is hydrogen bonded to N(Gly381) and O(Thr149). Analysis of the temperature factors of the mutant indicates a dramatic increase in the *B* factors for residues 147−163 of the loop domain (Figure 4), when compared to all the other biosynthetic thiolase structures. This region, in particular Leu148, closes the tight binding pocket of the fatty acid tail. The hydrogen bonding interactions of Gln64 are apparently important in anchoring this region of the loop domain to the bulk of the protein, which is possibly relevant for the very narrow substrate specificity of the enzyme (*12*). The high level of sequence conservation of Gln64 in synthetic thiolases

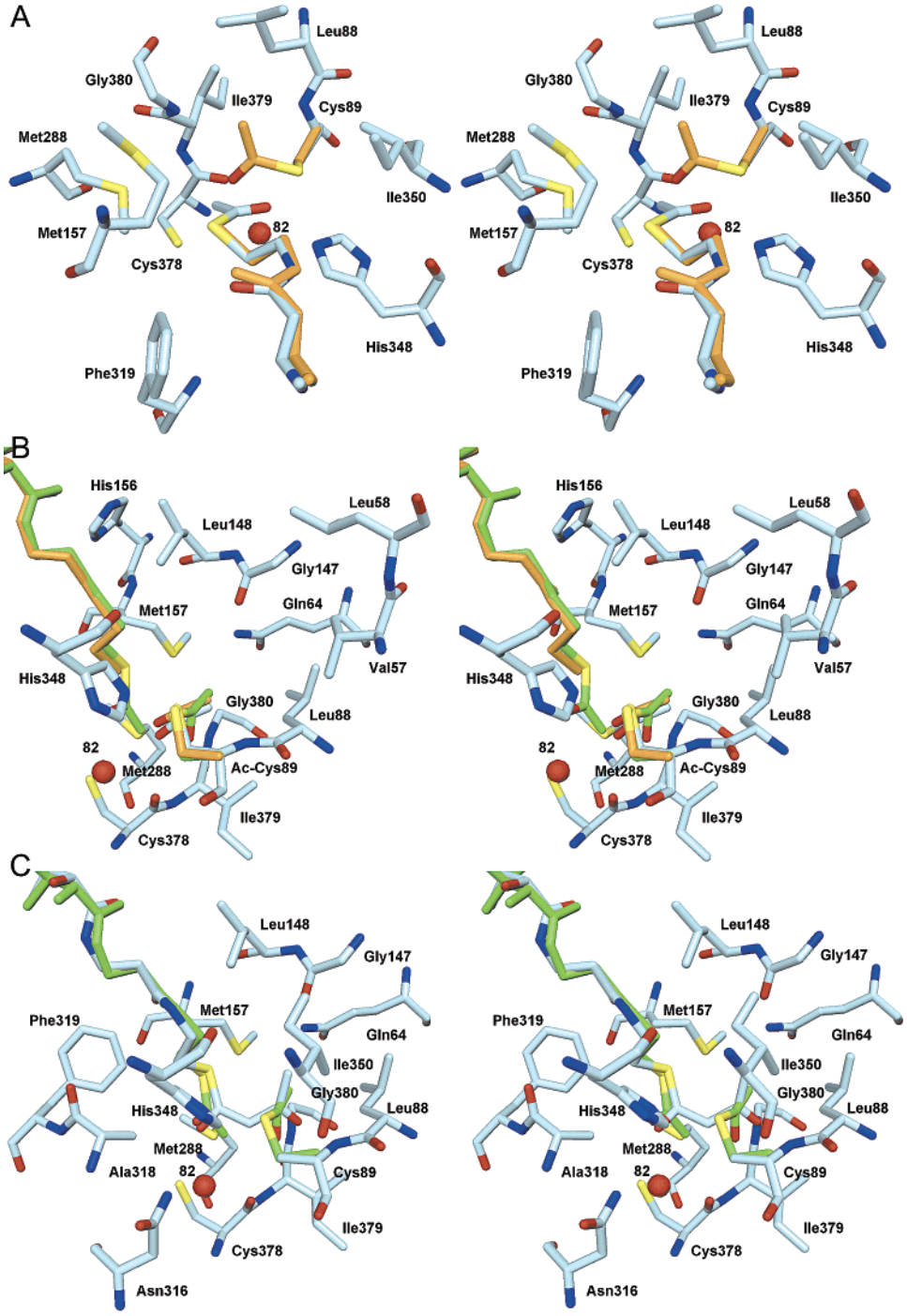

FIGURE 7: Visualization of the structural rearrangements taking place during the thiolase reaction cycle. The numbering scheme of the complexes is provided in Figure 2. (A) Structures of complexes 2 and 3 (top view). The carbon atoms of Cys89 and CoA in complex 3 are colored orange. These complexes represent the active site before and after transacetylation has occurred, respectively. From the orientation of the acetyl group on Ac-CoA in complex 2, it can be deduced that the negative charge developing on its O1 in the transition state is stabilized by the oxyanion hole formed by His348 and Wat82. (B) Orientation of the acetyl group on Cys89 in complexes 3−5. The entrance of Ac-CoA induces a movement in acetyl-Cys89 that brings its O1 into the oxyanion hole of N(Cys89) and N(Gly380). Complex 3 is indicated in orange and complex 5 in green. (C) Complexes 5 and 6. These complexes represent the structure before and after Claisen condensation, respectively. The thioester oxygen atoms that will be negatively charged in the transition states are in the oxyanion holes in both structures. Green carbon atoms represent complex 5.

suggests that this anchoring interaction is important for the function of biosynthetic thiolase.

DISCUSSION

General Aspects of the Thiolase Reaction and the Active Site. The thiolase reaction can be considered a cycle consisting of a series of six intermediates (Figure 2). In this cycle, two distinct chemical conversions are catalyzed; these reactions are an acyl transfer, where complex 2 is converted into complex 3, and a Claisen condensation, in which complex 5 is converted into complex 6. Thiolase can catalyze these conversions in both directions, i.e., toward the synthesis

or the degradation of AcAc-CoA. The bacterial thiolase discussed in this paper has evolved to function in a synthetic pathway; consequently, the catalytic events will be discussed here in this context. Thus, the first event of the catalytic cycle is the binding of Ac-CoA (Figure 2). Now, crystal structures are available that represent each of the six complexes of the reaction pathway, and a complete picture of the structural events occurring during the entire thiolase reaction cycle can be obtained.

The active site of biosynthetic thiolase is characterized by the presence of two reactive cysteine residues, Cys89 and Cys378. The active site catalyzes two chemically different reactions, both of which involve the transfer of an acetyl group between the enzyme and Ac-CoA. In the first reaction, the acetyl group is transferred between the sulfur atoms of CoA and Cys89; simultaneously, a proton is transferred from Cys378 to the S atom of the leaving group, CoA (Figure 2). In the second reaction, the acetyl group is transferred from the sulfur atom of Cys89 to the C2 atom of a second Ac-CoA molecule. At the same time, a proton is transferred from C2(Ac-CoA) to Cys378. In this reaction, also termed Claisen condensation, a C−C bond is formed between an electrophile, C1 of acetylated Cys89, and a nucleophile, C2 of Ac-CoA. Both of these carbon atoms belong to a thioester group, and the stabilization of the charges on these carbon atoms is favored by electrostatic interactions of the thioester oxygen atoms with two oxyanion holes. In these two reactions, Cys89 functions as a carrier of acetyl groups, and Cys378 shuttles protons.

Key factors determining the substrate specificity of biosynthetic thiolase are the size and properties of its substrate-binding pocket. The active-site cavity of biosynthetic thiolase is small and rigid, explaining the very narrow substrate specificity. For example, the k_{cat} values for the cleavage of C6−3-oxoacyl-CoA and 2-methyl−acetoacetyl-CoA are, respectively, less than 0.1% and nondetectable when compared to the reaction with AcAc-CoA (*12*). In the unliganded state, the active-site region contains no formally charged atoms. The active-site cavity has polar and apolar faces such that the center of the polar face of the active site is near Wat82, and the apolar face is formed by the side chains of Leu88, Ile350, Val57, Leu148, Met288, Met157, and Phe319. In the standard view (for example, Figures 3C and 6A), the polar face can be termed the bottom of the cavity, while the hydrophobic side chains form the ceiling of the cavity. In complex 6, AcAc-CoA is bound so that the hydrophobic S and C4 atoms point upward, contacting the hydrophobic face, while the O1 and O3 atoms of the substrate interact intimately with the polar face (Figures 3C and 6B). The tight packing of the active-site cavity is in agreement with the earlier observation that acetyl-dithio-CoA cannot acetylate the enzyme (*36*). The thiocarbonyl moiety in this compound is significantly more bulky than the oxocarbonyl group of Ac-CoA (*36*). The acetyl group is so tightly packed that there would not be enough space to exchange the carbonyl oxygen with a sulfur atom, considering the structure of the acetylated enzyme.

Two distinct oxyanion holes stabilize the two different transition states. The oxyanion hole functioning only in Claisen condensation is formed by the main chain nitrogen atoms of Cys89 and Gly380. Such oxyanion holes are also seen in serine proteases (*37*) and other enzymes, for example, esterases such as acetylcholinesterase (*38*). In serine proteases, the NH donor groups are provided by the same loop. In thiolase and acetylcholinesterase, the two NH groups are provided by two different loops; in these enzymes, the second NH group is donated by a glycine-rich loop, corresponding to the Gly380-Gly381-Gly382 sequence in thiolase. The other oxyanion hole in thiolase is formed by Wat82 and Nϵ2-(His348). This oxyanion hole stabilizes transition state intermediates of both the acyl transfer and Claisen condensation reactions.

It is further interesting to note that the thiolase active site is located at the N-termini of the two long central helices, Nα3 and Cα3, of the thiolase fold. Residues of the first turn of these helices contact each other, and a buried water molecule is bound in this region, hydrogen bonded to N(Ser91) and N(Gly92) of Nα3 and to N(Ser353) and N(Gly354) of Cα3. The helix dipoles (*39*) of these helices may be an important factor in the thiolase reaction. For example, the negatively charged oxyanions of the transition states point toward the N-termini of these helices. Also, an essential step of the thiolase reaction is the deprotonation of Sγ(Cys89), which will be favored by the positive electrostatic potential of the N-terminus of the Nα3 helix. The lowering of pK_a values of ionizing Cys residues by helical dipoles has been reported previously (*40*) and also suggested to play a role in the generation of a nucleophilic cysteine in another enzyme having the thiolase fold, FabH, from *E. coli* (*41*). The localization of Cys89 in a tight turn, stabilized by the hydrogen bond between the main chain carbonyl oxygen of the Ramachandran outlier Leu88 and the amide nitrogen of Ser91, as well as the one between Oγ of Ser91 and the main chain nitrogen of Gln87, may be important in enabling the Sγ atom to take full advantage of the helix dipole.

In the entire substrate-binding pocket, His348 is the only group having a transient positive charge; the only negative charges lie on either of the two active-site cysteines, depending on the stage of the reaction. During the course of the reaction, negatively charged transition states are formed that are stabilized either by the oxyanion hole of N(Cys89) and N(Gly380) or by the side chain of His348 and Wat82. The negative charge on Cys89 generated upon ligand binding (complexes 2 and 6) is transferred to Cys378 for the second half of the catalytic cycle (in complexes 3−5). The negative charge on Sγ(Cys378) is stabilized by hydrogen bonds to Wat82 and Wat49, which interact with His348 and a water channel, respectively. Thus, the transient positive charge on His348 will also effectively decrease the pK_a of Cys378, via Wat82. In fact, the nearest charge to Sγ(Cys378) is in the side chain of His348, 7 Å away. In the Claisen condensation step, when complex 5 is converted to complex 6, the protonation state of Cys378 reverts back to the neutral state.

Analysis of the crystal structures of all the intermediates of the thiolase reaction allows one to compare the atoms that move during the reaction cycle. Strikingly, the only protein atom, apart from protons, that moves during the entire thiolase reaction is the Sγ atom of Cys89. Once substrate binds, this atom moves closer to His348, at the same time being deprotonated. Then, it stays in the same position throughout all reaction steps, regardless of whether it is acetylated. In the unliganded structure, the Sγ(Cys89)−Nϵ2-(His348) distance is 4.2 Å; the small displacement of the Sγ atom upon substrate binding shortens this distance to 3.0

Å (Figure 6C). The other moving atoms during the reaction belong to the two acetyl groups brought into the active site by CoA, while the CoA moiety itself is always bound in the same mode. The first acetyl group that is brought into the active site by the first Ac-CoA molecule goes through four distinct conformations and two oxyanion holes before leaving the active site as the terminal acetyl group of AcAc-CoA (Figures 6 and 7). The only clear role played by solvent directly in the reaction mechanism is the stabilization by Wat82 of the two transition states in which the O1 atom of the substrate transiently has a negative charge.

Events Taking Place at the Active Site during the Biosynthetic Thiolase Reaction Cycle. If we consider the reaction along the synthetic pathway, the unliganded enzyme (complex 1) binds Ac-CoA (complex 2), and at the same time, the side chain of Cys89 rotates toward His348 (Figure 6C), as seen, for example, in the structure of the complex between unmodified thiolase and CoA (*20*). His348 activates Cys89 by abstracting the proton from its Sγ atom, creating a reactive nucleophile, at the same time acquiring a positive charge. O1 of the acetyl group in Ac-CoA is now hydrogen bonded to the oxyanion hole comprised of Wat82 and Nϵ2(His348).

In the acyl transfer step, the acetyl group is transferred from Ac-CoA to Cys89, during which the tetrahedral intermediate is stabilized by His348 and Wat82. Upon comparison of the active-site geometry of complex 2 with the structure of acetylated thiolase with CoA (complex 3), it is clear that the transfer of the acetyl group is accompanied by a major structural rearrangement of the acetyl group (Figure 7A), while the hydrogen bonding interaction between the thioester oxygen and Wat82 is maintained. The C1 atom of the acetyl group moves by 2.2 Å upon its transfer from CoA to Cys89. In the predicted tetrahedral transition state, in which the acetyl group is shared by the sulfur atoms of CoA and Cys89, the O1 atom of the acetyl group carries a negative charge. The orientation of the acetyl group in the structures indicates that the transient negative charge on the oxygen is stabilized by the His348 Nϵ2 atom, which has a positive charge as it previously has activated Cys89 for nucleophilic attack by abstracting the proton from its Sγ. Also, Wat82 is involved in the stabilization of the intermediate. The acyl transfer reaction is completed when the leaving group, CoA, is protonated by Cys378. The importance of this protonation reaction is emphasized by the significantly reduced reaction rate of the acylation step observed for a C378G mutant (*42*). From the available crystal structures, it is clear that the oxyanion hole formed by the main chain N atoms of Cys89 and Gly380 is not involved in the acyl transfer step.

The O1 atom of the acetyl group on Cys89 does not yet enter the other oxyanion hole, formed by N(Cys89) and N(Gly380), in the presence of CoA (complex 3). When CoA has left the active site (complex 4), the conformation of acetyl-Cys89 stays unchanged. When the second Ac-CoA molecule enters the active site of the acetylated enzyme (complex 5), it causes the rotation of the acetyl group on Cys89 so that its O1 atom now enters the oxyanion hole (Figure 7B). In fact, the dihedral angles (Cβ−Sγ−C1−O1) of the acetylated Cys89 for complexes 3−5 are 74°, 71°, and 28°, respectively, indicating that it is the entrance of Ac-CoA that drives the thioester oxygen on Cys89 into the oxyanion hole. In this strained conformation, the two acetyl moieties are stacked on top of each other at a distance of 3.0 Å and contacted by the negatively charged Sγ(Cys378) 3.3 Å away from C2 of Ac-CoA (Figure 7B,C). This geometry is in agreement with experimental studies showing that the stereochemistry of the reaction causes inversion at the methyl group of Ac-CoA that is converted to the methylene group in AcAc-CoA (*11*, *43*). Sγ(Cys378) is well-positioned for abstracting the C2 proton, allowing for the subsequent condensation reaction between the nucleophilic C2(Ac-CoA) and the electrophilic C1(Ac-Cys89) to proceed. The electrophilic character of this C1 atom is enhanced by the presence of the tight oxyanion hole formed by N(Cys89) and N(Gly380).

The Claisen condensation reaction is initiated by the loss of a proton from C2 of Ac-CoA to the Sγ atom of Cys378 (*42*). It is experimentally well established (*12*, *34*, *36*) that Cys378 is a more efficient catalytic base in the acetylated enzyme than in the apo form. In the complex between the acetylated enzyme and Ac-CoA (complex 5), the distance between Sγ of Cys378 and C2 of Ac-CoA is only 3.3 Å, while the distance between the corresponding atoms in complex 6 is 4.4 Å. Due to resonance, the carbonyl O1 of Ac-CoA has a partial negative charge, and hydrogen bonding with His348 Nϵ2 and Wat82, as seen in complexes 5 and 6 (Figure 7C), stabilizes this planar transition state intermediate. The C2 carbanion of Ac-CoA reacts with the electrophilic C1 atom of acetylated Cys89. The negative charge on the thioester oxygen atom of Ac-Cys89 of the tetrahedral intermediate is stabilized in the oxyanion hole formed by N(Cys89) and N(Gly380). After Claisen condensation, AcAc-CoA is present in the active site (complex 6), with its O3 oxygen still in the second oxyanion hole (Figure 5B). The O3 atom of AcAc-CoA points deep into the oxyanion hole, its distance to N(Cys89) being 3 Å and that to N(Gly380) being 2.5 Å. The loss of AcAc-CoA from the active site, and the simultaneous rotation of the Cys89 side chain to the apo position, completes the thiolase reaction cycle.

Two Water Channels Traverse through the Thiolase Fold from the Active Site. Previously, it was noted that an extensive water-mediated hydrogen bonding network, involving the buried charged residues Arg356 and Glu314, extends from the biosynthetic thiolase active site all the way to the backside of the subunit (*20*), but this network does not contact bulk solvent. Further examination has now indicated that, indeed, there also exists a water channel that connects the thiolase active site to bulk solvent on the backside of the protein (Figure 5). The previously observed water cluster, including the protein side chains, is conserved between synthetic and degradative thiolases (*2*, *20*), except for differences in some side chain conformations at the far end of the network. The water channel only exists in the synthetic enzyme; the corresponding space is filled by hydrophobic residues in the degradative enzyme. These water networks of biosynthetic thiolase pass through the thiolase fold on opposite sides of the same β-strand (Cβ2), and are both packed between a nearby helix and this β-strand. It is unclear how, and to what extent, these water channels may affect the catalytic properties of the thiolase active site. The present structures show that the first water molecule of the water channel, Wat82, is important in stabilizing negatively charged reaction intermediates in both the acyl transfer and Claisen condensation steps. In acyl transfer, this intermediate

is a tetrahedral species, while in the Claisen condensation, a planar enolate form of acetyl-CoA is involved.

CONCLUDING REMARKS

The crystallographic data allow for a detailed description of the structural events occurring during the catalytic cycle of biosynthetic thiolase. The mode of binding of the acetyl and acetoacetyl moieties is determined by hydrogen bonding interactions of the substrate oxygen atoms with polar atoms, as well as via van der Waals interactions with hydrophobic side chains. Once substrate has been bound, the actual catalytic cavity of biosynthetic thiolase is a very tightly packed environment. The size, shape, and polarity of this cavity are the key factors behind the substrate specificity of the enzyme. From the observed mode of binding of the substrates, it can be understood how Sγ(Cys89) can react with either C1 (acyl transfer) or C3 (Claisen condensation) of the substrate. Similarly, it can be rationalized that Sγ-(Cys378) can exchange protons with either S(CoA) (acyl transfer) or C2(Ac-CoA) (Claisen condensation). Thus, Cys89 and Cys378 have completely different catalytic properties. This correlates with the markedly different geometry of the two side chains. Cys89 is in an unstrained conformation, located at the N-terminus of the long central Nα3 helix. The nucleophilic character of Sγ(Cys89) is enhanced by the hydrogen bonding interactions of the Cys89-His348-Ser353 triad. Such catalytic triads (*44*) are also seen in serine and cysteine proteases, as well as in CoA-dependent enzymes other than thiolase. For example, catalytic triads such as this include the Ser-His-Asp triad in chymotrypsin, the Cys-His-Asn triad in papain, and the Cys-His-Asp triad in arylamine *N*-acetyltransferase (*45*). Cys378 is in a reverse turn between antiparallel β-strands β4 and β5 of the C-terminal half. The side chain χ_1 dihedral angle of Cys378 is approximately 60°. This is a strained conformation, usually not observed (*46*). Cys378 is not part of a catalytic triad; instead, it is hydrogen bonded to Wat82 and Wat49. These two water molecules are involved in extensive hydrogen bond networks, which are proposed to play a key role in determining the catalytic properties of biosynthetic thiolase.

ACKNOWLEDGMENT

We thank Wolfgang Kabsch for helpful discussions about data processing. The staff of beamline I711 at the MAX-Lab, the protein crystallography beamlines at EMBL-Hamburg/DESY, and beamline ID29 at EMBL-Grenoble are acknowledged for excellent support in data collection. We further thank Inari Kursula for data collection in Grenoble and Yorgo Modis for help during the initial stages of this study. We also thank Drs. Werner Schmitz and Jens Knudsen for stimulating discussions.

REFERENCES

1. Mishra, P. K., and Drueckhammer, D. G. (2000) Coenzyme A analogues and derivatives: synthesis and applications as mechanistic probes of coenzyme A ester-utilizing enzymes, *Chem. Rev. 100*, 3283−3310.
2. Mathieu, M., Modis, Y., Zeelen, J. P., Engel, C. K., Abagyan, R. A., Ahlberg, A., Rasmussen, B., Lamzin, V. S., Kunau, W. H., and Wierenga, R. K. (1997) The 1.8 Å crystal structure of the dimeric peroxisomal 3-ketoacyl-CoA thiolase of *Saccharomyces cerevisiae*: implications for substrate binding and reaction mechanism, *J. Mol. Biol. 273*, 714−728.
3. Modis, Y., and Wierenga, R. K. (1999) A biosynthetic thiolase in complex with a reaction intermediate: the crystal structure provides new insights into the catalytic mechanism, *Structure 7*, 1279−1290.
4. Staack, H., Binstock, J. F., and Schulz, H. (1978) Purification and properties of a pig heart thiolase with broad chain length specificity and comparison of thiolases from pig heart and *Escherichia coli*, *J. Biol. Chem. 253*, 1827−1831.
5. Bennett, M. J., Hosking, G. P., Smith, M. F., Gray, R. G., and Middleton, B. (1984) Biochemical investigations on a patient with a defect in cytosolic acetoacetyl-CoA thiolase, associated with mental retardation, *J. Inherited Metab. Dis. 7*, 125−128.
6. Ozand, P. T., Rashed, M., Gascon, G. G., al Odaib, A., Shums, A., Nester, M., and Brismar, J. (1994) 3-Ketothiolase deficiency: a review and four new patients with neurologic symptoms, *Brain Dev. 16*, 38−45.
7. Fukao, T., Scriver, C. R., and Kondo, N. (2001) The clinical phenotype and outcome of mitochondrial acetoacetyl-CoA thiolase deficiency (β-ketothiolase or T2 deficiency) in 26 enzymatically proved and mutation-defined patients, *Mol. Genet. Metab. 72*, 109−114.
8. Madison, L. L., and Huisman, G. W. (1999) Metabolic engineering of poly(3-hydroxyalkanoates): from DNA to plastic, *Microbiol. Mol. Biol. Rev. 63*, 21−53.
9. Jez, J. M., Bowman, M. E., and Noel, J. P. (2001) Structure-guided programming of polyketide chain-length determination in chalcone synthase, *Biochemistry 40*, 14829−14838.
10. Val, D., Banu, G., Seshadri, K., Lindqvist, Y., and Dehesh, K. (2000) Re-engineering ketoacyl synthase specificity, *Structure 8*, 565−566.
11. Walsh, C. T. (1979) Enzyme-catalyzed aldol and Claisen condensations, in *Enzymatic Reaction Mechanisms*, pp 773−776, W. H. Freeman and Co., San Francisco.
12. Masamune, S., Walsh, C. T., Sinskey, A. J., and Peoples, O. P. (1989) Poly-(R)-3-hydroxybutyrate (PHB) biosynthesis: mechanistic studies on the biological Claisen condensation catalyzed by β-ketoacyl thiolase, *Pure Appl. Chem. 61*, 303−312.
13. Kunau, W. H., Dommes, V., and Schulz, H. (1995) β-Oxidation of fatty acids in mitochondria, peroxisomes, and bacteria: a century of continued progress, *Prog. Lipid Res. 34*, 267−342.
14. Fukao, T., Song, X. Q., Mitchell, G. A., Yamaguchi, S., Sukegawa, K., Orii, T., and Kondo, N. (1997) Enzymes of ketone body utilization in human tissues: protein and messenger RNA levels of succinyl-coenzyme A (CoA):3-ketoacid CoA transferase and mitochondrial and cytosolic acetoacetyl-CoA thiolases, *Pediatr. Res. 42*, 498−502.
15. Thompson, S., Mayerl, F., Peoples, O. P., Masamune, S., Sinskey, A. J., and Walsh, C. T. (1989) Mechanistic studies on β-ketoacyl thiolase from *Zoogloea ramigera*: identification of the active-site nucleophile as Cys89, its mutation to Ser89, and kinetic and thermodynamic characterization of wild-type and mutant enzymes, *Biochemistry 28*, 5735−5742.
16. Williams, S. F., Palmer, M. A., Peoples, O. P., Walsh, C. T., Sinskey, A. J., and Masamune, S. (1992) Biosynthetic thiolase from *Zoogloea ramigera*. Mutagenesis of the putative active-site base Cys-378 to Ser-378 changes the partitioning of the acetyl S-enzyme intermediate, *J. Biol. Chem. 267*, 16041−16043.
17. Masamune, S., Palmer, M. A. J., Gamboni, R., Thompson, S., Davis, J. T., Williams, S. F., Peoples, O. P., Sinskey, A. J., and Walsh, C. T. (1989) Bio-Claisen condensation catalyzed by thiolase from *Zoogloea ramigera*. Active site cysteine residues, *J. Am. Chem. Soc. 111*, 1879−1881.
18. Tomita, K., Saito, T., and Fukui, T. (1983) Bacterial metabolism of poly-β-hydroxybutyrate, in *Biochemistry of metabolic processes* (Lennon, D. L. F., Stratman, F. W., and Zahlten, R. N., Eds.) pp 353−366, Elsevier Science, Amsterdam.
19. Gilbert, H. F., Lennox, B. J., Mossman, C. D., and Carle, W. C. (1981) The relation of acyl transfer to the overall reaction of thiolase I from porcine heart, *J. Biol. Chem. 256*, 7371−7377.
20. Modis, Y., and Wierenga, R. K. (2000) Crystallographic analysis of the reaction pathway of *Zoogloea ramigera* biosynthetic thiolase, *J. Mol. Biol. 297*, 1171−1182.
21. Cleland, W. W. (1963) The kinetics of enzyme-catalyzed reactions with two or more substrates or products. I. Nomenclature and rate equations, *Biochim. Biophys. Acta 67*, 104−137.

22. Middleton, B. (1974) The kinetic mechanism and properties of the cytoplasmic acetoacetyl-coenzyme A thiolase from rat liver, *Biochem. J. 139*, 109−121.
23. Laemmli, U. K. (1970) Cleavage of structural proteins during the assembly of the head of bacteriophage T4, *Nature 227*, 680−685.
24. Cerenius, Y., Ståhl, K., Svensson, L. A., Ursby, T., Oskarsson, Å., Albertsson, J., and Liljas, A. (2000) The crystallography beamline I711 at MAX II, *J. Synchrotron Radiat. 7*, 203−208.
25. Kabsch, W. (1993) Automatic processing of rotation diffraction data from crystals of initially unknown symmetry and cell constants, *J. Appl. Crystallogr. 26*, 795−800.
26. Brunger, A. T. (1992) Free R-value: a novel statistical quantity for assessing the accuracy of crystal structures, *Nature 355*, 472−475.
27. Murshudov, G. N., Vagin, A. A., and Dodson, E. J. (1997) Refinement of macromolecular structures by the maximum-likelihood method, *Acta Crystallogr. D53*, 240−255.
28. Collaborative Computational Project Number 4 (1994) The CCP4 Suite: Programs for Protein Crystallography, *Acta Crystallogr. D50*, 760−763.
29. Berman, H. M., Westbrook, J., Feng, Z., Gilliland, G., Bhat, T. N., Weissig, H., Shindyalov, I. N., and Bourne, P. E. (2000) The Protein Data Bank, *Nucleic Acids Res. 28*, 235−242.
30. Winn, M. D., Isupov, M. N., and Murshudov, G. N. (2001) Use of TLS parameters to model anisotropic displacements in macromolecular refinement, *Acta Crystallogr. D57*, 122−133.
31. Perrakis, A., Morris, R., and Lamzin, V. S. (1999) Automated protein model building combined with iterative structure refinement, *Nat. Struct. Biol. 6*, 458−463.
32. Laskowski, R. A., MacArthur, M. W., Moss, D. S., and Thornton, J. M. (1993) PROCHECK: a program to check the stereochemical quality of protein structures, *J. Appl. Crystallogr. 26*, 283−291.
33. Mathieu, M., Zeelen, J. P., Pauptit, R. A., Erdmann, R., Kunau, W. H., and Wierenga, R. K. (1994) The 2.8 Å crystal structure of peroxisomal 3-ketoacyl-CoA thiolase of *Saccharomyces cerevisiae*: a five-layered α β α β α structure constructed from two core domains of identical topology, *Structure 2*, 797−808.
34. Davis, J. T., Moore, R. N., Imperiali, B., Pratt, A. J., Kobayashi, K., Masamune, S., Sinskey, A. J., Walsh, C. T., Fukui, T., and Tomita, K. (1987) Biosynthetic thiolase from *Zoogloea ramigera*. I. Preliminary characterization and analysis of proton transfer reaction, *J. Biol. Chem. 262*, 82−89.
35. Davis, J. T., Chen, H. H., Moore, R., Nishitani, Y., Masamune, S., Sinskey, A. J., and Walsh, C. T. (1987) Biosynthetic thiolase from *Zoogloea ramigera*. II. Inactivation with haloacetyl CoA analogs, *J. Biol. Chem. 262*, 90−96.
36. Anderson, V. E., Bahnson, B. J., Wlassics, I. D., and Walsh, C. T. (1990) The reaction of acetyldithio-CoA, a readily enolized analog of acetyl-CoA with thiolase from *Zoogloea ramigera*, *J. Biol. Chem. 265*, 6255−6261.
37. Kraut, J. (1977) Serine proteases: structure and mechanism of catalysis, *Annu. Rev. Biochem. 46*, 331−358.
38. Ordentlich, A., Barak, D., Kronman, C., Ariel, N., Segall, Y., Velan, B., and Shafferman, A. (1998) Functional characteristics of the oxyanion hole in human acetylcholinesterase, *J. Biol. Chem. 273*, 19509−19517.
39. Hol, W. G., van Duijnen, P. T., and Berendsen, H. J. (1978) The α-helix dipole and the properties of proteins, *Nature 273*, 443−446.
40. Kortemme, T., and Creighton, T. E. (1995) Ionisation of cysteine residues at the termini of model α-helical peptides. Relevance to unusual thiol pK_a values in proteins of the thioredoxin family, *J. Mol. Biol. 253*, 799−812.
41. Davies, C., Heath, R. J., White, S. W., and Rock, C. O. (2000) The 1.8 Å crystal structure and active-site architecture of β-ketoacyl-acyl carrier protein synthase III (FabH) from *Escherichia coli*, *Structure 8*, 185−195.
42. Palmer, M. A., Differding, E., Gamboni, R., Williams, S. F., Peoples, O. P., Walsh, C. T., Sinskey, A. J., and Masamune, S. (1991) Biosynthetic thiolase from *Zoogloea ramigera*. Evidence for a mechanism involving Cys-378 as the active site base, *J. Biol. Chem. 266*, 8369−8375.
43. Willadsen, P., and Eggerer, H. (1975) Substrate stereochemistry of the acetyl-CoA acetyltransferase reaction, *Eur. J. Biochem. 54*, 253−258.
44. Dodson, G., and Wlodawer, A. (1998) Catalytic triads and their relatives, *Trends Biochem. Sci. 23*, 347−352.
45. Sandy, J., Mushtaq, A., Kawamura, A., Sinclair, J., Sim, E., and Noble, M. (2002) The structure of arylamine *N*-acetyltransferase from *Mycobacterium smegmatis*: an enzyme which inactivates the anti-tubercular drug, isoniazid, *J. Mol. Biol. 318*, 1071−1083.
46. Richardson, J. S., and Richardson, D. C. (1989) Principles and patterns of protein conformation, in *Prediction of protein structure and the principles of protein conformation* (Fasman, G. D., Ed.) pp 1−98, Plenum Press, New York.
47. Kraulis, P. J. (1991) MOLSCRIPT: A program to produce both detailed and schematic plots of protein structures, *J. Appl. Crystallogr. 24*, 946−950.
48. Philippsen, A. (2001) DINO: Visualizing structural biology, http://www.dino3d.org.
49. Sanner, M. F., Olson, A. J., and Spehner, J. C. (1996) Reduced surface: an efficient way to compute molecular surfaces, *Biopolymers 38*, 305−320.

BI0266232